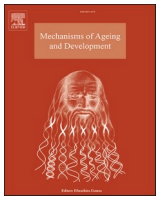
Mechanisms of Ageing and Development 225 (2025) 112064



Contents lists available at ScienceDirect

Mechanisms of Ageing and Development

journal homepage: www.elsevier.com/locate/mechagedev





Differential effects of lifespan-extending genetic manipulations in an animal model of MJD/SCA3

Marta Daniela Costa [a,b], Jorge Diogo Da Silva [a,b], Dulce Almeida [a,b], Joana Pereira-Sousa [a,b], Daniela Vilasboas-Campos [a,b], Jorge Humberto Fernandes [a,b], Andreia Teixeira-Castro [a,b,1], Patrícia Maciel [a,b,1,*]

[a] Life and Health Sciences Research Institute (ICVS), School of Medicine, University of Minho, Braga 4710-057, Portugal
[b] ICVS/3Bs - PT Government Associate Laboratory, Guimarães, Braga, Portugal

ARTICLE INFO

Keywords:
Aging
C. elegans
MJD/SCA3
Insulin/IGF-1
Mitochondrial dysfunction
Dietary restriction
Germline signaling

ABSTRACT

Aging is a natural biological process, but evidence suggests that some aspects of aging can be delayed and reduce the prevalence of neurodegenerative diseases, for which aging is a key risk factor. In a neuronal *Caenorhabditis elegans* model of a Polyglutamine disease-Spinocerebellar Ataxia Type 3 (SCA3), or Machado-Joseph disease (MJD)- we assessed the hypothesis that delaying aging is neuroprotective, investigating the effect of genetically manipulating multiple lifespan-determinant mechanisms. Lifespan-increasing mutations causing insulin/IGF-1 signaling downregulation, mitochondrial dysfunction, germline ablation and dietary restriction/innate immune activation had distinct impacts on MJD/SCA3 phenotypes, suggesting that not all genetic strategies of stalling aging are equally neuroprotective and challenging the idea that delaying aging is a guaranteed therapy for these diseases. Lifespan-extension improved the SCA3/MJD motor phenotype only when induced by altered nutrient-sensing pathways such as those mediated by insulin/IGF-1 and *eat-2* signaling, but their effects on neuronal aggregation differed. These pathways exhibited differential proteostasis profiles, but both activated the heat shock response suggesting that they operate through partially independent mechanisms to confer neuroprotection. The therapeutic value of the insulin/IGF-1 downregulation was demonstrated through the chronic treatment of the SCA3/MJD model with an insulin/IGF-1 signaling inhibitor, underscoring the relevance of aging manipulations in guiding therapeutic strategies for these diseases.

1. Introduction

Neurodegenerative diseases are progressive and debilitating conditions that remain without any effective disease-modifying therapy and are therefore associated with profound socioeconomic and personal/family implications. Aging, considered a key risk factor for the emergence of these disorders, (Hou et al., 2019) has been shown to be particularly amenable to manipulation, and aging-delaying interventions were shown to slow progression of some diseases, either by retarding the toxic process that leads to neurodegeneration or through the activation of neuroprotective mechanisms.

In *C. elegans*, a significant extension in lifespan can be achieved by several environmental manipulations and by genetic alterations in mechanisms of aging regulation, (Kenyon, 2010) that change the signaling cascades of the following genetic pathways: i) the insulin/insulin-like growth factor (IGF-1) signaling (IIS) pathway. The loss-of-function of the *C. elegans* receptor, *daf-2*, or downstream alterations in its signaling cascade, cause a dramatic increase in animals' lifespan (Kenyon et al., 1993). The reduction of insulin/IGF-1 signaling culminates in the translocation of the transcription factor DAF-16/FOXO to the nucleus, where it controls the expression of several genes linked with proteostasis, metabolism and resistance to different stressors (Murphy and Hu, 2013). Additional elements seem to cooperate with DAF-16, such as the heat-shock factor 1 (HSF-1), a transcription factor known to orchestrate the heat-shock response), PQM-1 (a relatively uncharacterized GATA zinc-finger transcription factor) and SKN-1/NRF2 (a master transcriptional regulator of the oxidative and xenobiotic stress response) (Tullet et al., 2008; Uno and Nishida, 2016).

* Correspondence to: Life and Health Sciences Research Institute (ICVS), School of Medicine, University of Minho, Gualtar Campus, Braga 4710-057, Portugal.
E-mail address: pmaciel@med.uminho.pt (P. Maciel).
[1] # These authors contributed equally to the work

https://doi.org/10.1016/j.mad.2025.112064
Received 27 February 2025; Received in revised form 4 April 2025; Accepted 21 April 2025
Available online 24 April 2025
0047-6374/© 2025 The Author(s). Published by Elsevier B.V. This is an open access article under the CC BY-NC-ND license (http://creativecommons.org/licenses/by-nc-nd/4.0/).

ii) Dietary restriction (DR) pathway. DR can be defined as limited food intake without causing malnutrition. It is able to dramatically increase the lifespan of different eukaryote species (McCay et al., 1989), mostly by downregulating mTOR signaling. Additional players are implicated in DR-mediated longevity, depending on the diet regimen and the timing of food deprivation. DAF-16/FOXO, SKN-1/NRF2 and PHA-4/FOXA are the most well-known downstream targets of the mTOR/DR cascade, essentially impacting the antioxidant response, autophagy and mRNA translation (Mair and Dillin, 2008; Panowski et al., 2007). The loss-of-function of *eat-2* has long been recognized as a genetic model of DR, as it reduces pharyngeal pumping, limiting food intake. However, recent studies indicate that alterations in innate immunity also play a crucial role in mediating the longevity effects observed in *eat-2* mutants (Wu et al., 2019; Kumar et al., 2019).iii) Mitochondrial dysfunction. Reactive oxygen species (ROS), mainly generated in mitochondria, were initially regarded as the main cause of cellular damage and aging (referred to as the free radical theory of aging) (Harman, 2003). However, the isolation of long-lived *C. elegans* mutants with mild mitochondrial perturbations in the electron transport chain and increased levels of ROS was a significant breakthrough on the understanding of the pro-longevity role of moderate levels of ROS (Lee et al., 2003; Feng et al., 2001). As with other aging-related pathways, several factors and processes seem to be required for the mitochondria-associated increment in longevity, namely SKN-1/NRF2, HIF-1, autophagy, and even the involvement of DAF-16/FOXO was recently proposed (Lee et al., 2010; Hwang and Lee, 2011; Senchuk et al., 2018). iv) Germline function. The removal of germline cells also increases lifespan in worms through the key mediator DAF-12/PXR/VDR which acts together with DAF-16/FOXO, SKN-1/NRF2, NRH-80/HNF4, NHR-49/PPARα, HLH-30/TFEB and PHA-4/FOXA, resulting in changes in fatty acid metabolism as well as enhanced autophagy and proteasome activity (Arantes-Oliveira et al., 2002; Hsin and Kenyon, 1999; Antebi, 2013; Qin and Hubbard, 2015; Goudeau et al., 2011; O'Rourke and Ruvkun, 2013; Ratnappan et al., 2014).

The premise that aging might influence the onset and progression of neurodegenerative diseases has motivated studies where genetic approaches were used to delay aging in disease models. Experiments in *C. elegans* models of proteotoxicity-associated diseases such as Alzheimer's disease, ALS/FTD and polyglutamine diseases showed the protective effect of insulin/IGF-1 signaling and dietary manipulations (Zhang et al., 2011; Cohen et al., 2006; Teixeira-Castro et al., 2011a; Morley et al., 2002). In these models, lifespan-extending mutations in components of the insulin/IGF-1 pathway delayed the onset of PolyQ-mediated toxicity and aggregation in muscle and this effect was shown to be mediated by HSF-1 and DAF-16 (Cohen et al., 2006; Teixeira-Castro et al., 2011a; Steinkraus et al., 2008). Different DR regimens also suppressed proteotoxicity, albeit with variable impacts in the toxic accumulation of aggregation-prone proteins (Morley et al., 2002; Steinkraus et al., 2008; Matai et al., 2019). More recently, the first investigation on the role of multiple lifespan-increasing mutations in *C. elegans* neuronal models of genetic and sporadic Parkinson's disease, (Senchuk et al., 2021; Cooper et al., 2015) has suggested a largely neuroprotective role of distinct aging manipulation strategies against dopaminergic neuronal damage. This research is of particular translational relevance, as neurons are the primary focus of interest. Nevertheless, similar investigations in the context of other neurodegenerative diseases are still required to understand whether such strategies can be therapeutic options for diverse diseases. Equally important is the need to explore the pathways downstream of these longevity regulators and identify those amenable to drug targeting.

Polyglutamine (PolyQ) diseases are neurodegenerative diseases caused by unstable CAG repeat expansions in the coding regions of distinct genes. As result, the translated proteins present an abnormal structure due to the presence of a larger tail of glutamine residues that promotes their aggregation in neurons, causing dysfunction and, ultimately, death (Fan et al., 2014; Paulson, 2012; Bettencourt and Lima, 2011; Lieberman et al., 2019). Despite the disease-causing proteins being expressed since birth in patients, PolyQ diseases are adult-onset conditions. It suggests that in addition to the CAG repeat length- the main disease determinant, (Maciel et al., 1995) aging is also a primary risk factor for this disease.

In this study, we explored in a neuronal model of proteotoxicity, the potential of several anti-aging genetic manipulations as modifiers of neurodegenerative processes. The neuroprotective effect of distinct lifespan-increasing mutations targeting insulin/IGF-1, DR, mitochondrial dysfunction and germline signaling were investigated in a *C. elegans* model of one of the most common PolyQ diseases worldwide - Machado-Joseph disease, also known as spinocerebellar ataxia type 3 (SCA3) (Teixeira-Castro et al., 2011a). To more specifically determine whether alterations in the proteostasis network are linked to effective pro-longevity changes in the context of this disease, and whether beneficial genetic backgrounds share similar mechanisms, we evaluated the gene expression of key components within this network. Finally, we assessed whether pharmacological interventions that mimic the most effective aging-delaying mechanism in the *C. elegans* model of MJD/SCA3 could be therapeutic options for this disease, with translational potential to patients.

2. Results

2.1. Longevity-associated mutations increase the lifespan of the C. elegans model of MJD/SCA3

We first explored the impact of different longevity-promoting mutations on the lifespan of the *C. elegans* model of MJD/SCA3 (AT3q130). This model expresses a full-length mutant human ataxin-3 protein with 130 glutamines, under a pan-neuronal promoter, and shows motor impairments and neuronal protein aggregation. The lifespan of transgenic animals (Teixeira-Castro et al., 2011a) was significantly increased by all studied aging-related mutations: in *daf-2*, the unique insulin/IGF-1 receptor in *C. elegans* (Fig. 1A); *clk-1* and *isp-1* (Fig. 1B-C) which respectively encode a protein needed for ubiquinone biosynthesis and a Rieske iron sulphur subunit of the mitochondrial complex III (both impacting mitochondrial function); *glp-1*, a highly conserved LIN-12/Notch family of receptors that affects germline proliferation and confers sterility (Fig. 1D), and in *eat-2*, whose mutation causes pharyngeal pumping deficits, innate immune activation, bacterial avoidance and dietary restriction (Fig. 1E).

However, the extent of lifespan increase of the MJD model was different for the various mutations: ~14.6 days for *daf-2* mutation, ~1.7 days if mutated for *isp-1*, ~2 days in the case of alterations in *clk-1* and *eat-2,* and ~3.6 days when germline proliferation was blocked (Table S1). The lifespan extension brought by the lifespan-enhancing mutations was comparable to the corresponding genetic mutant alone, the exception being *isp-1* and *eat-2* whose double mutant lived significantly less than the corresponding single mutant (Fig. 1; Table S1). This different was pronounced and consistent in the case of *isp-1* alteration. We hypothesize that the combination of intrinsic mitochondrial dysfunction caused by *isp-1,* along with a potential imbalance in serotonergic signaling and oxidative status in AT3q130 animals, may jointly surpass a threshold beyond which the organism is no longer able to compensate for the degree of damage, leading to a decrease of lifespan when compared with *isp-1* single mutant. Considering that mitochondrial mutants are pleiotropic, it may be a mutation-specific effect. The mutation in insulin/IGF-1 receptor *daf-2* stood out as causing the highest impact in the disease model, almost doubling its mean lifespan.

2.2. Lifespan-increasing mutations modify mutant ATXN3 aggregation in C. elegans

Aggregation of mutant ATXN3 in neurons is a key hallmark of disease, which is recapitulated in an age-dependent manner in the

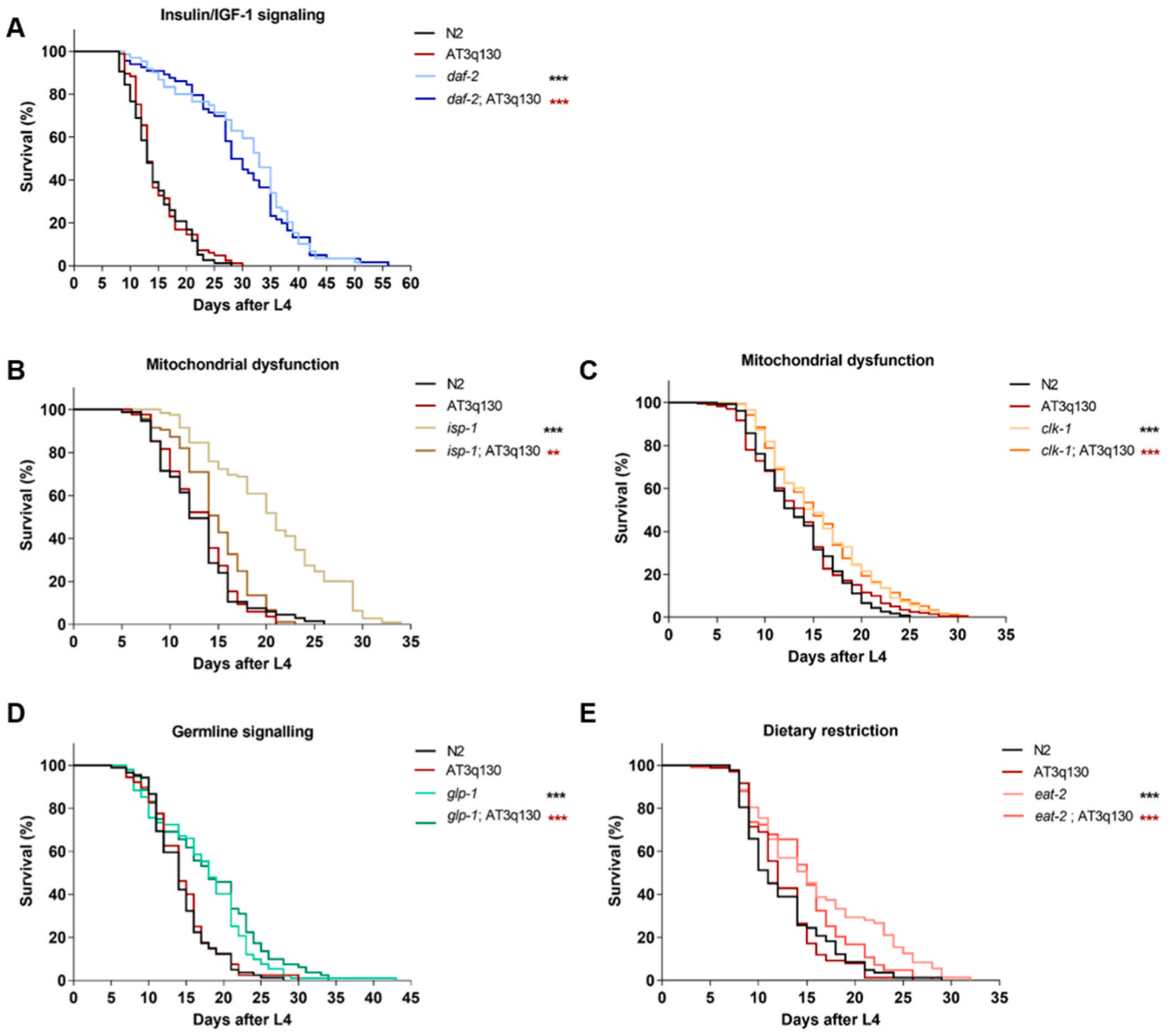


Fig. 1. Anti-aging genetic mutations increase the lifespan of the *C. elegans* model of MJD/SCA3. Kaplan-Meier representative survival curves of AT3q130 animals and double mutants: A) *daf-2 (e1370)*; AT3q130 B) *isp-1 (qm150)*; AT3q130 C) *clk-1 (e2519)*; AT3q130 D) *glp-1 (e2141)*; AT3q130 and E) *eat-2 (ad1113)*; AT3q130. Survival curves of the long-lived and short-lived controls *daf-2 (e1370)* and *daf-16 (mu86)*, respectively, were removed from the final graphs to allow better visualization of the results. *$p \leq 0.05$, * *$p \leq 0.01$, * **$p \leq 0.001$ (Kaplan-Meier Log-rank test). Black asterisks represent statistical comparison with N2 and dark red asterisks the difference to AT3q130 (H10 line for all mutants except for *eat-2* double mutant which was always compared with the P5 line – additional explanation in methods section). Detailed statistical parameters are described in Table S1.

AT3q130 model (Figure S1). This pathological finding can be easily monitored by the fluorescent YFP signal associated with mutATXN3 expression (Teixeira-Castro et al., 2011a). mutATXN3 aggregation in neurons of the animals' heads was quantified in AT3q130 animals and in double mutants through confocal microscopy, at days 4, 5 and 7 of adulthood (Fig. 2). We observed that all longevity-associated mechanisms modified the mutant ATXN3 aggregation in these neurons: genetic alterations in *daf-2*, *clk-1, isp-1* and *glp-1* significantly reduced the aggregation measures along animals' adulthood; however, this effect seemed more evident for *daf-2* and *isp-1* mutants. On the contrary, the *eat-2* mutation resulted in an increased mutATXN3 aggregation at all timepoints of observation.

To investigate whether the impact of lifespan-regulating mutations on mutATXN3 aggregation were due to potential alterations in the amount of mutATXN3 in the double mutants, we measured mutant ATXN3 transgene mRNA expression and the steady state levels of the mutant proteins, by RT-qPCR and Western blot, respectively (Figure S2). Notwithstanding some variability noticed in the expression of mutATXN3 transgene, the double mutants did not exhibit a significantly different level of mutATXN3 protein, suggesting that varying quantities of mutant protein are not mediating the phenotypic impact of these mutations. However, a trend for higher mutATXN3 mRNA and protein levels was observed in the *eat-2;* AT3q130 animals, which may have contributed to the observed increase in mutATXN3 aggregation.

Overall, this data demonstrated that the majority of the lifespan-increasing mutations modulates aggregation of the MJD-causing protein, but not through a major impact on its steady-state cellular levels.

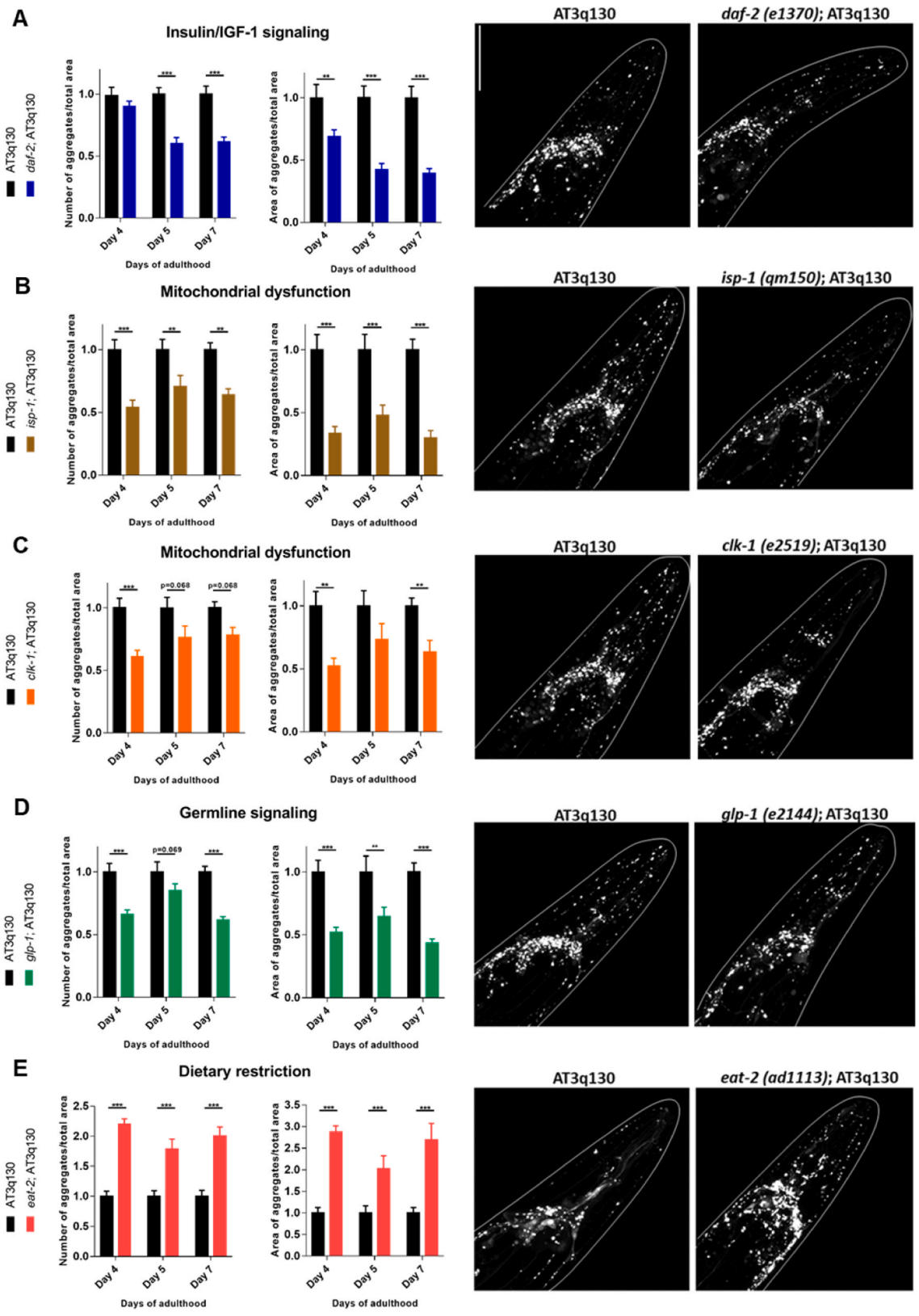


Fig. 2. Lifespan-increasing mutations are modifiers of mutATXN3 neuronal aggregation in the *C. elegans* model of MJD/SCA3. Graphs represent the number and area occupied by mutATXN3 aggregates in the neurons of the animals' head, corrected by the area of the head and normalized to the respective control. Neuronal mutATXN3 aggregation profiles were evaluated at days 4, 5 and 7 of adulthood in the *C. elegans* model of MJD/SCA3 and in each double mutant: A) *daf-2 (e1370)*; AT3q130 B) *clk-1 (e2519)*; AT3q130C) *glp-1 (e2141)*; AT3q130 and D) *eat-2 (ad1113)*; AT3q130. Data show mean values of aggregation measures corresponding to 2–3 independent assays per timepoint (N = 6–8 animals/assay) and error bars are SEM. *p ≤ 0.05, * *p ≤ 0.01, * **p ≤ 0.001 (Multiple *t*-test followed by Holm-Sidak correction method). Representative confocal images of animals at day 7 of adulthood are also shown. A scale bar of 50 μm is represented in the first picture.

2.3. Mutant ATXN3 neurotoxicity is differentially impacted by aging-delaying mechanisms

Next, we focused on the effect of the lifespan-increasing mutations on a key feature of the human disease, the progressive motor impairment, which is also recapitulated in the *C. elegans* model (Teixeira-Castro et al., 2011a). The presence of a *daf-2* mutation improved the motor performance of AT3q130 worms (Fig. 3A). This evidence validated our previous results that demonstrated the beneficial impact of this mutation (and of others in the same signaling cascade) in the motor phenotype of the same animals (Teixeira-Castro et al., 2011a), and it is in accordance with several other studies in distinct disease contexts that show the effectiveness of the insulin/IGF-1 inhibition in the reduction of proteotoxicity (Zhang et al., 2011; Cohen et al., 2006; Morley et al., 2002; Senchuk et al., 2021; Cooper et al., 2015). In contrast, AT3q130 animals harboring a lifespan-increasing mutation in the *e2519* allele of *clk-1* or a blockage of germline proliferation via *glp-1* mutation, although presenting an extended lifespan, did not recover from their motor deficits (Fig. 3B-C). In the case of the temperature-sensitive germline mutant background, this observation was also confirmed when motility was assessed after a 24 h recovery period at a permissive temperature (Figure S3). Evaluation of other mitochondrial long-lived mutants, namely the *isp-1* mutated background, was hindered by the significant motor impairment already verified for the single mutant.

On the other hand, an improved motor performance of AT3q130 animals was also attained by introducing the *eat-2* in the genetic background of the AT3q130 model (Fig. 3D), with double mutants showing significantly less locomotion deficits.

The *eat-2* mutation, introduced in a different genetic line of the MJD/

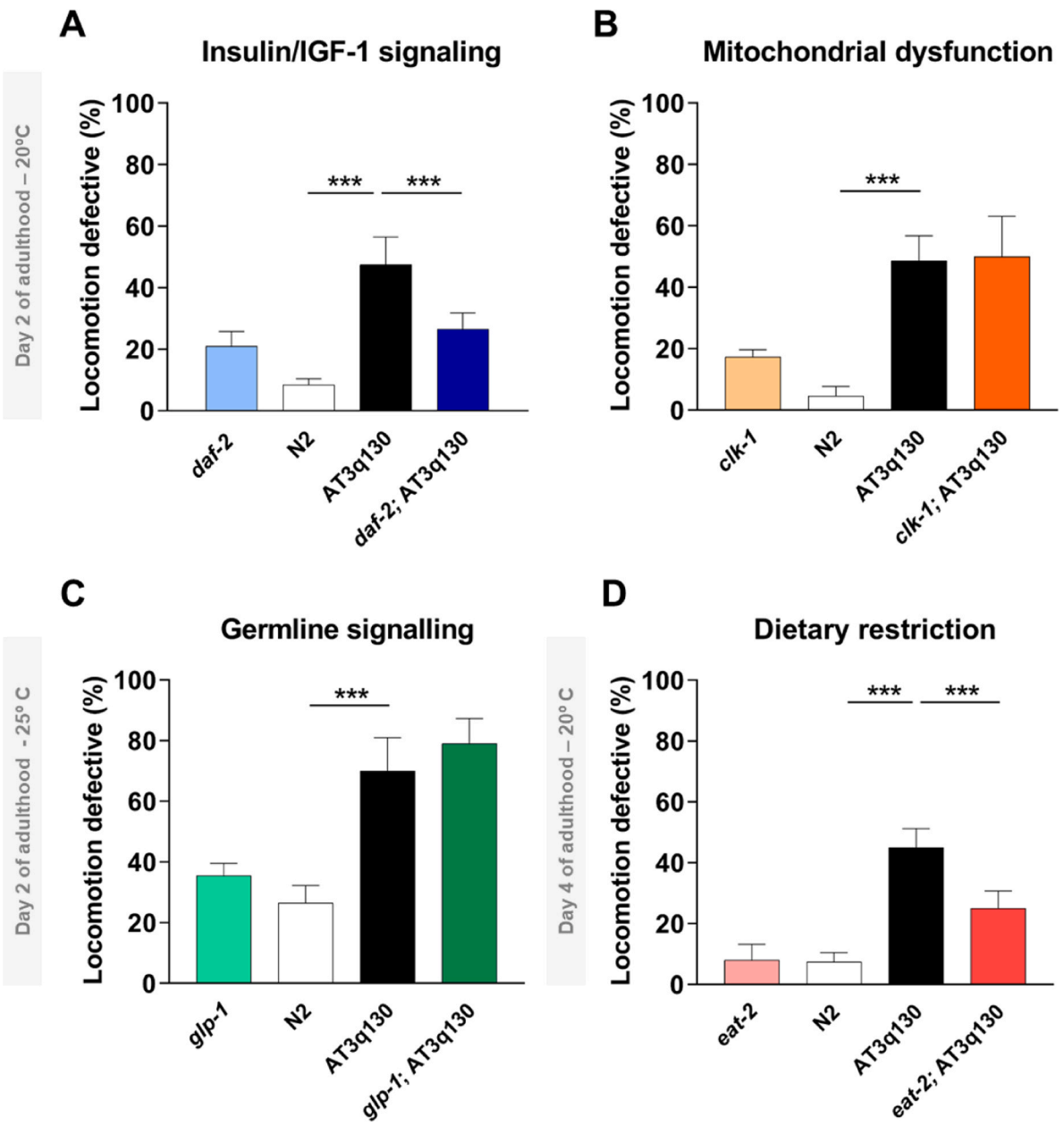


Fig. 3. Not all aging-delaying mutation ameliorate the motor symptoms in the *C. elegans* model of MJD/SCA3. Graphs represent the percentage of locomotion impairment of AT3q130 and double mutants: A) *daf-2 (e1370)*; AT3q130 B) *clk-1 (e2519)*; AT3q130C) *glp-1 (e2141)*; AT3q130 and D) *eat-2 (ad1113)*; AT3q130. The timepoints of behavioral evaluation and the animals' growth temperature is also indicated. Graphs show mean values of 3–4 independent assays (N = 50 animals/assay) and error bars correspond to SD. *p ≤ 0.05, * *p ≤ 0.01, * **p ≤ 0.001 (One-way ANOVA followed by Dunnet's multiple comparison test). See also Fig. S1.

SCA3 model (P5 line; additional information in methods details), caused a reduction of the motor phenotype of the model, even in presence of an unexpected increment in visible mutATXN3 aggregation. The impact of the silencing of this gene was further evaluated in the *C. elegans* model of MJD/SCA3 used in the rest of this work (H10 line), using feeding RNA interference (RNAi). Having confirmed the expected decrease of pharyngeal pumping upon *eat-2* silencing (Fig. 4A), we then verified that indeed, *eat-2* RNAi-mediated knockdown improved the motility of AT3q130 animals (Fig. 4B), in this case without causing significant alterations in the number and area of mutATXN3 aggregates of head neurons (Fig. 4C). Taken together, these results validate the modifier effect of *eat-2* alteration on mutATXN3 toxicity, adding to the suggestion of an uncoupling between motor phenotype and mutATXN3 aggregation.

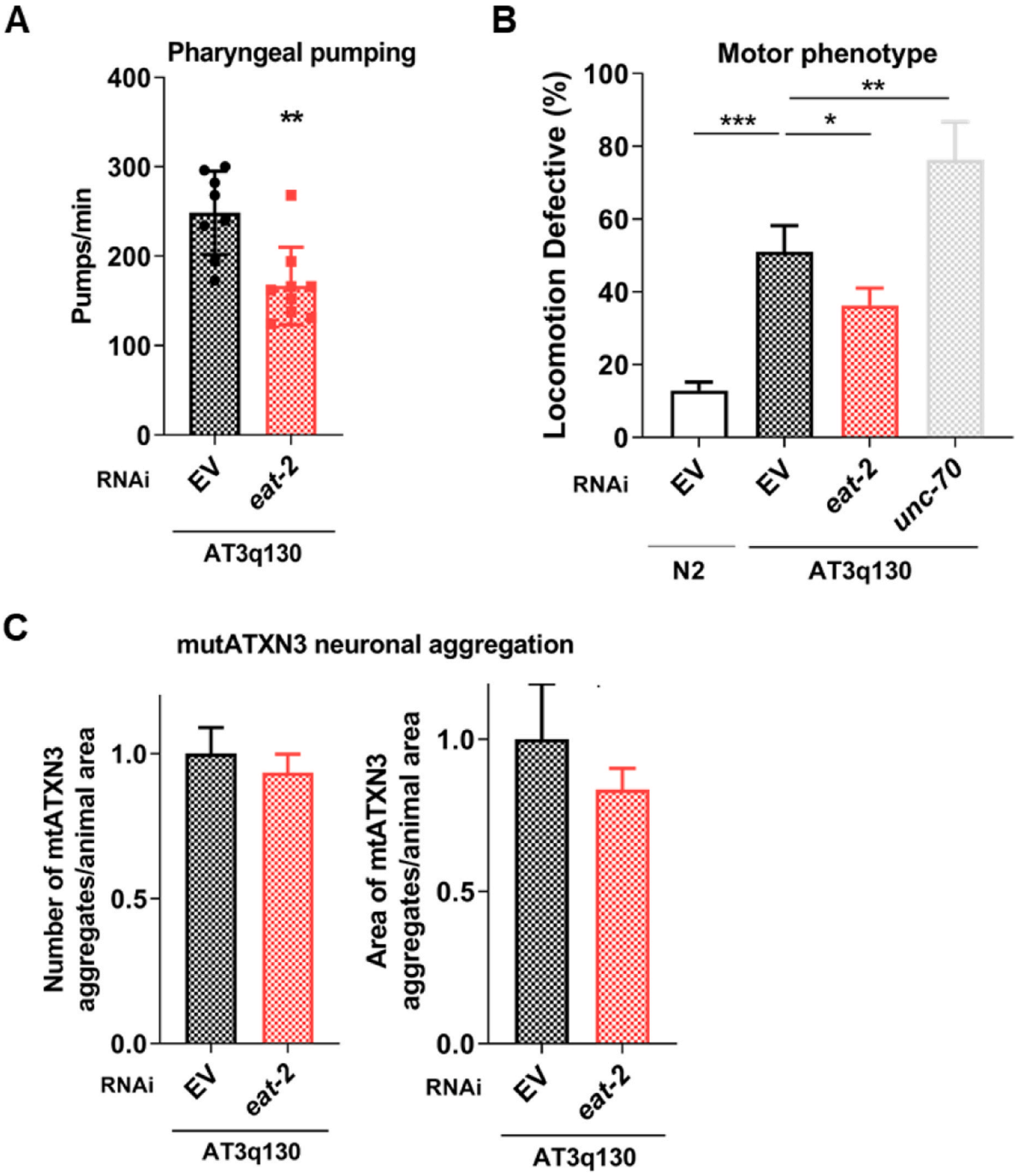


Fig. 4. RNAi-mediated silencing of *eat-2* in the *C. elegans* model of MJD/SCA3 improves motor function without affecting the mutATXN3 neuronal aggregation pattern. A) Pharyngeal pumping (pumps per minute) at day 2 of adulthood, in animals grown in empty vector (EV) and *eat-2* bacterial clones. Data show mean values of a representative assay (N = 9 animals per condition) and error bars are SD. *p ≤ 0.05, * *p ≤ 0.01, * **p ≤ 0.001 (Mann-Whitney test). B) Motor phenotype of the *C. elegans* model of MJD/SCA3, at day 2 of adulthood grown in empty vector (EV), *eat-2* and *unc-70* (positive control) bacterial clones. Data represent mean values of 4 independent assays (N = 50 animals/assay) and error bars are SD. *p ≤ 0.05, * *p ≤ 0.01, * **p ≤ 0.001 (One-way ANOVA followed by Dunnet's multiple comparison test). C) mutATXN3 neuronal aggregation, at day 4 of adulthood, in the *C. elegans* model of MJD/SCA3 grown in empty vector and *eat-2* bacterial clones. Graphs represent the number and the total area of aggregates present in the neurons of animal heads (corrected by the head area), normalized to the control. Data represent mean values of a representative assay (N = 7 animals). Statistical comparison between conditions by unpaired t test.

Overall, our data showed that in AT3q130 animals, not all genetic strategies that delay aging can improve the motor phenotype of the *C. elegans* model of MJD/SCA3, and those different strategies lead to different degrees of improvement. Nevertheless, mutations impacting nutrient sensing-related signaling pathways such as those associated with insulin/IGF-1 and *eat-2*, had a protective effect.

2.4. Pro-longevity mutations in daf-2 and eat-2 are associated with a distinct expression profile of molecular chaperones

Although some of these longevity-associated pathways have broad effects and their precise mechanisms are not yet fully understood, their potential to reshape protein quality control systems - challenged by both the presence of the disease-associated aggregation-prone protein and aging - could be highly significant. This modulation may help slow the age-related decline in proteome homeostasis (proteostasis), potentially influencing disease severity and providing insights into new therapeutic targets. To investigate whether protective pro-longevity genetic modifications lead to notable changes in the dynamics of proteostasis network components, and to determine if they operate through similar or distinct mechanisms, we conducted a transcriptomic analysis of key elements within the protein quality control systems. (Fig. 5). We assessed AT3q130 animals with either *daf-2* or *eat-2* mutation for protein degradation (proteasomal subunits *pbs-6* and *rpn-12*, and autophagy inducer *unc-51*/ULK1/ATG1 as markers) and protein folding pathways (representative classes of molecular chaperones: *hsp-1*; *hsp-110* (HSP-70); *dnj-12* (HSP-40) and *daf-21* (HSP90)).

Except for restoration of *pbs-6* levels induced by the *eat-2* mutation, no other significant alterations suggestive of key changes at the cellular degradation systems were associated with *daf-2* and *eat-2* mutations (Fig. 5A-B). However, in these double mutants, the expression profiles of factors associated with protein folding showed an interesting pattern: the expression of some molecular chaperones was decreased in AT3q130 animals with the *daf-2* mutation, when compared to the original MJD/SCA3 background, with this downregulation reaching statistical significance for *daf-21* (HSP90) and *hsp-110* (HSP-70). In contrast, upon mutation of *eat-2*, expression levels of *hsp-110* (HSP-70) and *dnj-12* (HSP-40) were increased (Fig. 5C).

These results revealed a contrasting expression profile of these molecular chaperones between the two disease-beneficial genetic backgrounds. This difference may reflect their distinct abilities to effectively modulate protein folding and aligns with their varying effects on mutATXN3 neuronal aggregation. Notably, a reduction in aggregation is only observed upon inhibition of the insulin/IGF-1 pathway (Fig. 2; Fig. 4).

2.5. Lifespan-increasing mutations in daf-2 and eat-2 activate overlapping stress-responsive pathways

Imbalances in protein homeostasis can be countered by organelle-specific stress responses (Yoneda et al., 2004; Zhao et al., 2002). To evaluate these branches of the protein quality control network, we measured the expression levels of: i) two key chaperones involved in the mitochondrial stress response, also known as mitochondrial unfolded protein response (^{mt}UPR): *hsp-6*, the mitochondrial hsp-70 heat-shock protein family member, and *hsp-60*, the mitochondrial GroE/hsp60/hsp10chaperonin family member (Fig. 6A); ii) a chaperone of the endoplasmic reticulum unfolded protein stress response (^{ER}UPR): *hsp-3* (Fig. 6B); iii) distinct inducible hsp-70 (C12C8.1 and F44E5.4) and small heat-shock proteins (hsp-16 family) involved in the cytosolic heat-shock response (HSR) (Fig. 6C).

Whenever present in the genetic background of the *C. elegans* model of MJD/SCA3, the mutations in *eat-2* and *daf-2* were associated with non-overlapping transcriptomic profiles regarding some of these stress responses, as is the case of ^{mt}UPR and ^{er}UPR, the first showing to be downregulated only in *daf-2* double mutants and the latter demonstrating a significant increase in expression of its marker *hsp-3* only in *eat-2* double mutants (Fig. 6 A, B). On the other hand, both pro-longevity mutations seem to upregulate several genes related with the HSR (more evident in *daf-2;* AT3q130 animals), albeit the full clarification of these profiles was hampered by the variable expression of these highly responsive genes and the consequent lack of statistical significance of some apparent differences (Fig. 6C).

These findings suggested that both pro-longevity mutations can activate partially overlapping cellular stress responses and lead us to hypothesize that the similar shared transcriptomic changes seen in the

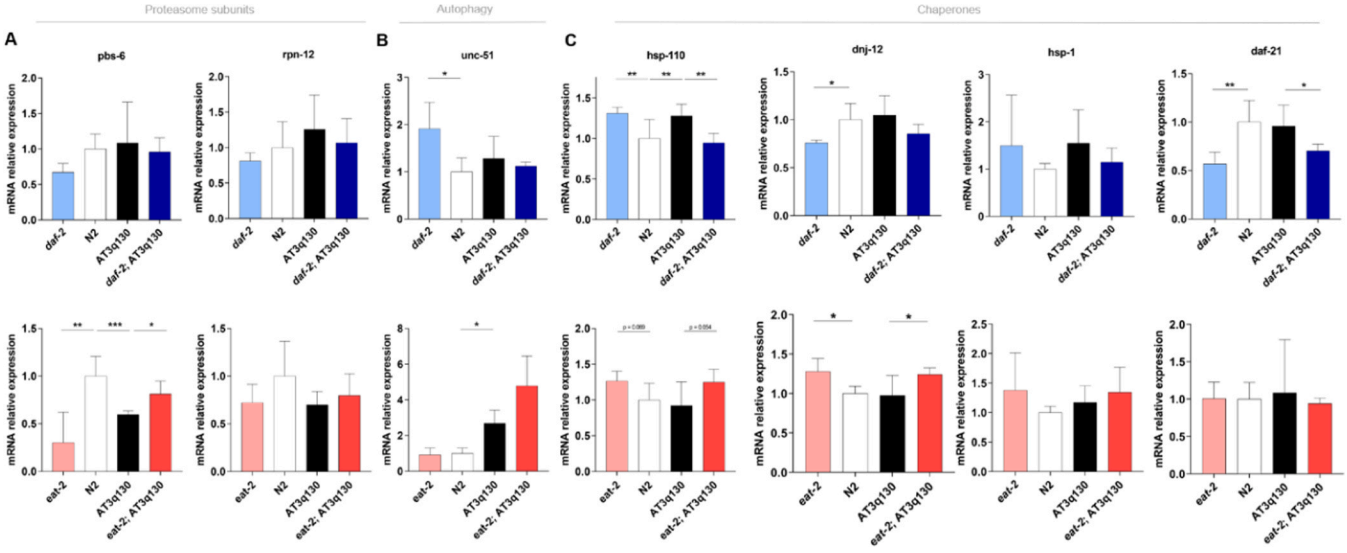


Fig. 5. Alterations in the insulin/IGF-1 signaling and in dietary restriction-mediated signaling are associated with distinct alterations in the expression levels of molecular chaperones. Graphs represent relative mRNA expression levels at day 2 of adulthood, of two proteasome subunits, one marker of autophagy and several molecular chaperones: A) *daf-2 (e1370)*; AT3q130 B) *isp-1 (qm150)*; AT3q130C) *clk-1 (e2519)*; AT3q130 D) *glp-1 (e2141)*; AT3q130 and E) *eat-2 (ad1113)*; AT3q130. Data represent mean mRNA expression values, relatively to *rpb-2* and *pmp-3* housekeeping genes and normalized to the N2 WT strain; error bars correspond to the SD. For each genotype, a minimum of 4 biological and 2 technical replicates were considered. *p ≤ 0.05, * *p ≤ 0.01, * **p ≤ 0.001 (One-way ANOVA followed by planned orthogonal contrasts).

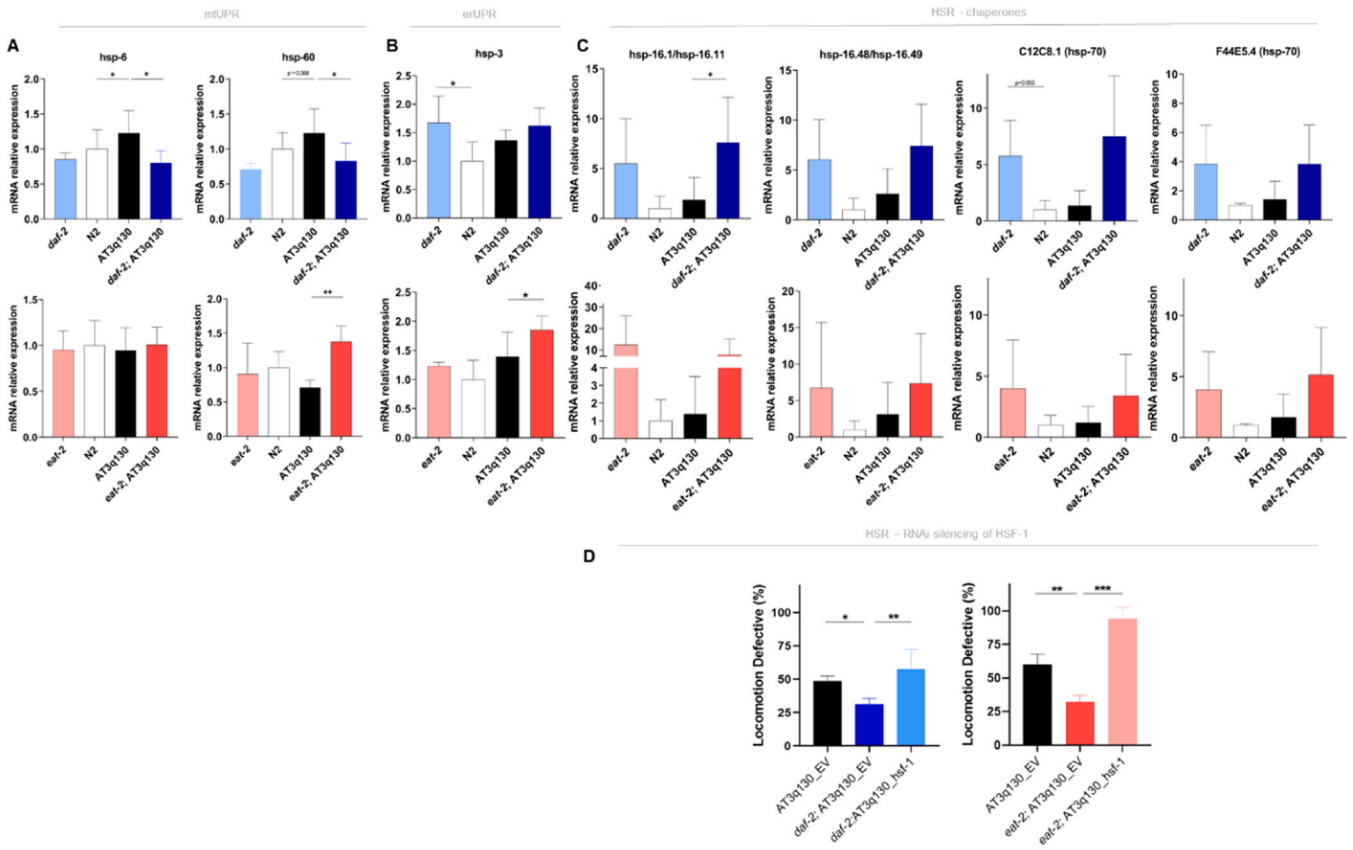


Fig. 6. Pro-longevity alterations mediated by *daf-2* and *eat-2* mutations recruit partially overlapping alterations in HSR and ^{ER}UPR stress responses. Graphs represent relative mRNA expression levels at day 2 of adulthood, of A) *hsp-6* and *hsp-60*; B) *hsp-3;* C) *hsp-16.1/hsp-16.11*; *hsp16–48/hsp-16.49*; C12C8.1 and F44E5.4 (inducible hsp70s), in *daf-2* and in *eat-2* mutants. Data represent mean mRNA expression values, relatively to *rpb-2* and *pmp-3* housekeeping genes and normalized to the N2 WT strain; error bars correspond to the SD. For each genotype, a minimum of 4 biological and 2 technical replicates were considered. *p ≤ 0.05, * *p ≤ 0.01, * **p ≤ 0.001 (One-way ANOVA followed by planned orthogonal contrasts). D) Motor phenotype of *daf-2 (e1370);* AT3q130 and *eat-2 (ad1113);* AT3q130 upon RNAi-mediating silencing of the master regulator of heat-shock response, HSF-1, at day 2 and 4 of adulthood, respectively The motility graph represents mean values of locomotion impairment after 3 independent assays (N = 50 animals/assay) and error bars are SD. *p ≤ 0.05, * *p ≤ 0.01, * **p ≤ 0.001 (One-way ANOVA followed by Dunnet's multiple comparison test).

HSR in *daf-2* and *eat-2* double mutants can be relevant to explain their common protective effect on the neuronal function of the *C. elegans* model of MJD/SCA3. The fact that expression levels of HSR-related small heat shock proteins were unchanged in the *clk-1* double mutants (Figure S4), in which the pro-longevity effect were unable to improve the animals' motor phenotype (Fig. 3), favored the hypothesis that HSR-activation (or small heat-shock proteins such as hsp-16 more specifically) could be correlated with the neuroprotective effect of *daf-2* and *eat-2* mutations. To further clarify this hypothesis, the transcription factor HSF-1, which is the master regulator of the heat-shock response, was silenced by RNAi in *daf-2*; AT3q130 and *eat-2*; AT3q130 animals (Fig. 6D). Upon HSF-1 silencing, the motor improvements observed in both mutants were reversed, supporting the hypothesis that the heat-shock response is influenced by both lifespan-extending mutations in the MJD/SCA3 model and contributes to the motor benefits associated with these variants.

2.6. The downregulation of insulin/IGF-1 signaling promotes an antioxidative state in the C. elegans model of MJD/SCA3

After evaluating several branches of the proteostasis network, we carried out a similar analysis regarding oxidative stress response-related pathways. The inhibition of the insulin/IGF-1 signaling, via *daf-2* mutation, caused a significant upregulation of antioxidant enzymes such as *gst-10*, *sod-3* and *ctl-1/ctl-2* in the *C. elegans* model of MJD/SCA3. Of note, that these changes were mostly absent in DR animals (Fig. 7A). The involvement of key transcription factors that regulate the antioxidant response was also investigated: we focused on SKN-1/NRF-2, a mediator of adaptative cellular responses to oxidative stress and other insults, namely its isoform b (exclusively expressed in ASI neurons) and isoforms a and c (which instead respond to distinct stimuli in intestine), (Blackwell et al., 2015) and NHR-57, a well-known target gene of the hypoxia-inducible factor (HIF-1), also activated by reactive oxygen species (ROS) through a currently unknown mechanism (Fig. 7B) (Lee et al., 2010). We observed a recovery of SKN-1/NRF-2 isoforms a/c expression in the *eat-2* double mutant, while in *daf-2*; AT3q130 animals expression of this transcription factor is kept induced as in the AT3q130 animals. On the other hand, the levels of the neuronal isoform of SKN-1/NRF-2, although undistinguishable between WT and the MJD model, were strongly up-regulated by both longevity-associated mechanisms, suggesting that, in neurons, SKN-1/NRF-2 is commonly recruited by distinct longevity-associated mechanisms. Similarly, the expression of NHR-57 was increased in the long-lived mutants, albeit without reaching statistical significance in the *eat-2* double mutants.

The functional relevance of these transcriptomic changes was assessed by submitting animals with reduced insulin/IGF-1 signaling and *eat-2*-mediated alterations - conditions with distinct antioxidant expression profiles, to an oxidative stress resistance assay. Our results suggest that the transcriptomic alterations in *daf-2* double mutants do result in a protective state against oxidative stress, as the *daf-2* mutation, but not the *eat-2* mutation, was able to strongly protect AT3q130 animals from juglone-induced oxidative damage (Figure S5 A).

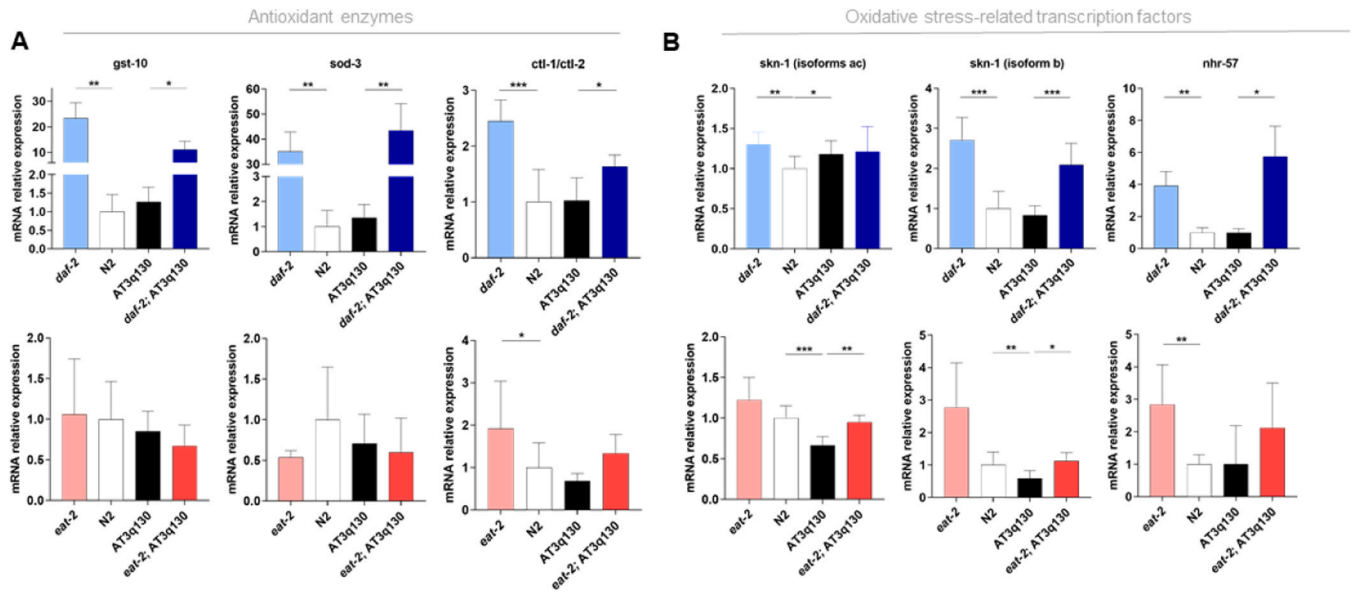


Fig. 7. The reduction of insulin/IGF-1 signaling is associated with an antioxidant gene expression profile in the *C. elegans* model of MJD/SCA3. Graphs represent relative mRNA expression levels, of A) distinct antioxidant enzymes: *sod-3*, *gst-10* and *ctl-1/ctl-2* and B) oxidative-stress associated transcription factors: *Skn-1/Nrf-2*, intestinal isoforms a and c, neuronal isoform b and *nhr-57*. Data represent mean mRNA expression values relatively to *rpb-2* and *pmp-3* housekeeping genes and normalized to the control N2; error bars correspond to the SD. For each genotype, a minimum of 4 biological and 2 technical replicates were considered. *p ≤ 0.05, * *p ≤ 0.01, * **p ≤ 0.001 (One-way ANOVA followed by planned orthogonal contrasts).

Despite significant transcriptomic changes in antioxidant response markers, namely in *daf-2* mutants, these changes do not appear to be central to the observed improvements in disease phenotypes. We also found an upregulation of *skn-1*, *nhr-57*, and antioxidant enzymes in the *glp-1;* AT3q130 strain, yet this double mutant did not show improvements in the motor phenotype compared to the AT3q130 disease model (Figure S5 B, C). Further investigation into the role of antioxidant enzymes in the *daf-2*; AT3q130 strain, by silencing *gst-10* and *sod-3*, showed no impact on its motor phenotype or on mutant ATXN3 aggregation (Figure S5 D). Additionally, crossing the *C. elegans* model of MJD/SCA3 with a strain that contains multiple copies of a PCR fragment containing the entire *ctl-1*, *ctl-2*, and *ctl-3* gene cluster (Doonan et al., 2008) to increase catalase activity did not produce a statistically significant phenotypic effect (Figure S5 E). Overall, these results suggest that although oxidative stress-related markers show significant changes, these alterations are not essentially responsible for the improvement in disease phenotypes.

2.7. Pharmacological inhibition of insulin/IGF-1-receptor supports the therapeutic value of manipulating this aging-delaying mechanism

While two anti-aging genetic strategies were neuroprotective in the AT3q130 model, the downregulation of the insulin/IGF-1 via *daf-2* knockout caused the most significant impact on key aspects of this

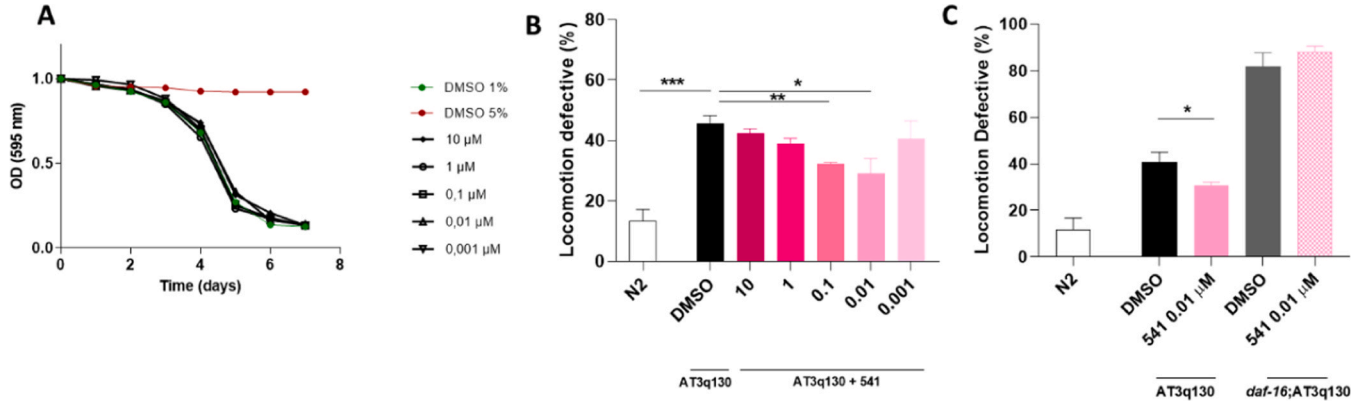


Fig. 8. Pharmacological inhibition of the insulin/IGF-1 receptor with compound NVP-AEW541 improve significantly the motor deficits of the *C. elegans* model of MJD/SCA3. A) Toxicity assay in WT animals treated with distinct concentrations of NVP-AEW541 showed no toxic effects based on the daily rate of food consumption (OD_{595}) and visual inspection. Animals treated with DMSO 1 % and 5 % were used as non-toxic and toxic controls, respectively. Curves in the graphs represent daily $OD_{595\ nm}$ values of five replicates, normalized for the $OD_{595\ nm}$ at day 0. Application of a non-linear regression model for sigmoidal curves, in DMSO 1 % and the distinct concentrations of each compound, fit a single model for LogIC50 and HillSlope values, indicative of no statistically significant differences between the curves (NVP-AEW541 p value = 0.33). B) At specific concentrations, NVP-AEW541 significantly improved the motor deficits of the *C. elegans* model of MJD/SCA3. Graphs represent the percentage of locomotion impairment of AT3q130 animals treated with several concentrations of the compound. Data show mean values of 4–5 independent assays (N = 50 animals/assay) and error bars are SD. *p ≤ 0.05, * *p ≤ 0.01, * **p ≤ 0.001 (One-way ANOVA followed by planned orthogonal contrasts) C) Impact of NVP-AEW541 in the motor phenotype of the *C. elegans* model of MJD/SCA3 upon *daf-16* mutation. Graphs represent the percentage of locomotion impairment of AT3q130 and *daf-16 (mu86);* AT3q130, treated with 0.01 µM of NVP-AEW541. Data show mean values of 3–4 independent assays (N = 50 animals/assay) and error bars are SD. *p ≤ 0.05, * *p ≤ 0.01, * **p ≤ 0.001 (Two-way ANOVA).

disease, namely lifespan, motility and mutATXN3 toxic accumulation. Taking this into account, and on the basis of the high degree of genetic/functional conservation of this signaling pathway to higher organisms, we explored its value as a potential translatable therapeutic target for MJD. For that, we pharmacologically modulated the insulin/IGF-1 pathway, using a small molecule inhibitor of IGF-1R tyrosine kinase activity (NVP-AEW541), previously tested as a potential anti-tumor agent (Arcaro, 2013; Haisa, 2013).

When used to treat WT *C. elegans*, NVP-AEW541 did not cause toxicity at a concentration range between 0.001 and 10 μM (Fig. 8A). Interestingly, chronic treatment of AT3q130 nematodes, at some of these concentrations, significantly improved the locomotion deficits of the animals (Fig. 8B), recapitulating the effect of the genetic mutation in the IGF-1R orthologue *daf-2*.

In the *C. elegans* model of MJD/SCA3, the knockout of *daf-16*, the primary transcriptional effector of the insulin/IGF-1 signaling pathway, resulted in a significant worsening of the motor phenotype. Although severe, previous studies have shown that this phenotype can be reversed by specific drug treatments (Teixeira-Castro et al., 2011a). In this study, the absence of DAF-16 in AT3q130 animals blocked the effectiveness of chronic treatment with NVP-AEW541, which had been previously observed. This suggests that DAF-16 is crucial for the biological activity of this compound, indicating that its effects are mediated through reduced insulin/IGF-1 signaling (Fig. 8C). The effective concentration of NVP-AEW541, 0.01 μM, did not impact the mutant ATXN3 aggregation load in animals, at the beginning of adulthood (Figure S6). Future studies will focus on detecting other aggregation species and examining additional timepoints. These findings support the conclusion that the insulin/IGF-1 pathway, which modulates aging, represents a druggable target and could provide effective therapeutic strategies for MJD/SCA3.

3. Discussion

Building on the premise that aging is a major risk factor for neurodegenerative diseases, we sought to investigate whether various genetic manipulations that influence aging progression—such as the reduction of insulin/IGF-1 signaling, alterations in mitochondrial function, changes in germline signaling, and modulation of food consumption—could confer protection in the context of neurodegenerative disorders. In addition to identifying the specific pathways associated with these protective effects, our study aimed to explore the potential for pharmacological strategies targeting these pathways as a means to combat neurodegeneration.

In MJD and in other spinocerebellar ataxias, the loss of motor function and coordination are key disabling symptoms in patients. From the studied aging-manipulation strategies, only the downregulation of the insulin/IGF-1 signaling and the dietary restriction/innate immune alterations caused by *eat-2* mutation ameliorated the motor abnormalities of the animals. The involvement of a reduced insulin/IGF-1 signaling in cellular detoxification events has previously been addressed in different *C. elegans* models of neurodegenerative diseases, mostly through muscle expression of disease-causing proteins, requiring the transcriptional function of HSF-1 and DAF-16 (Zhang et al., 2011; Cohen et al., 2006; Teixeira-Castro et al., 2011a; Morley et al., 2002). In the same line, the suppressor effect of food deprivation and genetic forms of diet restriction was also demonstrated in other *C. elegans* models of proteotoxicity (Steinkraus et al., 2008).

Regarding another disease hallmark, the neuronal aggregation of mutATXN3, we also observed a significant decrease in aggregates in the *C. elegans* model of MJD/SCA3 harboring the majority of lifespan-increasing mutations, albeit to different extents. The exception was the *eat-2*-mediated pathway, which did not reduce misfolded ATXN3-derived aggregates, despite correcting the locomotion impairment of the model. This implies an uncoupling between the effects on aggregation and motor behavior. This uncoupled impact was previously seen in drug screenings using the same model, (Teixeira-Castro et al., 2015; Pohl et al., 2019) and is in agreement with literature reports of similar observations in other models of neurodegenerative disorders (Lee et al., 2015).

Taken together, our results corroborate previous findings highlighting the neuroprotective role of aging-modulator nutrient-sensing mechanisms, specifically those related to insulin/IGF-1 signaling or mediated by *eat-2*, but we add that, despite extending lifespan, not all of the genetic mutations than prolong age were able to correct the motor deficits, a key hallmark phenotype of this model and patients. While the first study on the effects of multiple lifespan-extending changes in a *C. elegans* model of Parkinson's disease suggested broad neuroprotection conferred by such alterations, (Senchuk et al., 2021) albeit with distinct magnitudes of protection depending on the gene, our findings in a MJD model—which more accurately mimics the neuronal expression of the disease-causing mutant ATXN3— showed that not all lifespan-increasing mutations are neuroprotective. This challenges the assumption that aging-delaying genetic manipulations are universally effective in addressing age-related neurodegenerative diseases. Concordantly, both studies identified the insulin/IGF-1 signaling and *eat-2* mediated alterations as neuroprotective, with insulin/IGF-1 downregulation providing the greatest protection.

Although beneficial, the pattern of neuroprotection resulting from mutating *daf-2* and *eat-2* in the *C. elegans* model of MJD/SCA3 was distinct. Different effects have also been specifically attributed to each signaling pathway. For example, the aging-associated decline in neurotransmitters levels (and the resulting age-related behaviors) was rescued under environmental and genetic protocols of DR, but not in *C. elegans* with reduced insulin/IGF-1 signaling (Yin et al., 2014). Conversely, insulin/IGF-1 signaling, but not DR, affected age-dependent neurite branching in mechanosensory and motor *C. elegans* neurons (Tank et al., 2011). This evidence suggests that the two pathways operate through partially independent signaling cascades: (Steinkraus et al., 2008) Additionally, it is consensual that *eat-2*-mediated effects are largely independent of DAF-16, (Steinkraus et al., 2008) the key effector of the insulin/IGF-1 pathway. In our study, a distinct transcriptomic profile of several proteostasis network markers was observed between *daf-2* and *eat-2* double mutants: while a remarkable transcriptional activation of antioxidant enzymes and an overall downregulation of some constitutive and inducible chaperones was detected in *daf-2* mutants, in the presence of the *eat-2* mutation some constitutive chaperones were up-regulated. This differential gene expression further highlights the complex, pathway-specific effects of these longevity-related mutations and their impact on proteostasis, which likely contribute to their distinct neuroprotective effects in MJD/SCA3. However, it is also known that the reduction of insulin/IGF-1 signaling and genetic forms of chronic food deprivation share metabolic and transcriptomic changes, (Gao et al., 2018) as both may converge to the HSF-1 transcription factor. The hypothesis that HSF-1 activation can underlie the motor benefits upon *daf-2* and *eat-2* silencing in the *C. elegans* model of MJD/SCA3 seems plausible and it is supported by our results, which show a similar transcriptomic profile of HSR genes in both mutants, as well as the loss of motor improvements when their master regulator, HSF-1 is downregulated. Additionally, we previously demonstrated that chronic treatment with 17-DMAG, an HSP-90 inhibitor that activates the HSF-1-mediated heat shock response, improved the motor phenotype in the *C. elegans* model of MJD/SCA3, in a *daf-16*-independent manner (Teixeira-Castro et al., 2011a). Overall, we hypothesize that enhanced proteostasis underlies the protective effect of *daf-2* and *eat-2* mutations in AT3q130 animals, with a more pronounced effect in *daf-2* mutants, possibly due to its broader remodeling of the proteostasis network. However, the similar activation of the heat shock response (HSR) stress-response by insulin/IGF-1 reduction and *eat-2* alteration—suggesting that, although largely independent, both can recruit common downstream effectors—is a key finding. This shared activation likely contributes to their common protective effect on the motility of the model, which is a key hallmark of this disease.

The degree to which mechanisms underlying longevity differ and/or converge in common effectors has been also an intense topic of debate. Recently, a study that assessed commonalities of the transcriptomic profiles of *daf-2* and *isp-1* mutants highlighted the role of DAF-16/FOXO as a common mediator of longevity in both aging-regulating mechanisms, which were originally thought to be distinct (Senchuk et al., 2018). Thus, DAF-16/FOXO is not only an effector of the insulin/IGF-1 and germline ablation signaling cascades, but it is also required for mitochondria-associated longevity pathways. In our study, the fact that all longevity mechanisms leading to decreased mutATXN3 aggregation are known to be dependent on DAF-16/FOXO leads us to propose that additional key proteotoxicity-modifying factors could be identified among DAF-16/FOXO target genes.

Considering the efficacy of the inhibition of the insulin/IGF-1 signaling in the *C. elegans* model of MJD/SCA3 and also the high degree of functional conservation of this pathway to higher organisms, we also explored its therapeutic potential, repurposing an extensively studied inhibitor of IGF-1R autophosphorylation (Xue et al., 2012). Chronic treatment of AT3q130 animals with an IGF-1R kinase inhibitor robustly improved their motor abnormalities in a DAF-16/FOXO-dependent manner. Similar cancer-targeting compounds are already in clinical trials, demonstrating safety and promising results in cancer patients, (King and Wong, 2012) a fact that encourages additional studies of insulin/IGF-1 targeting compounds in pre-clinical models of neurodegenerative diseases. Our successful results using a IGF-1R kinase inhibitor adds to similar therapeutic strategies of insulin/IGF-1 reduction studied in *C. elegans* models of polyQ and Alzheimer's diseases, (El-Ami et al., 2014) reinforcing this as a druggable pathway and potential novel therapeutic target for many neurodegenerative diseases.

4. Conclusion

This study focuses on the specific effects of lifespan-increasing mutations in a model of PolyQ disease, rather than assuming a generalized benefit from delaying aging and thus postponing symptom onset. It adds complexity to our current understanding of the relationship between longevity and neurodegeneration by demonstrating that the beneficial effects of insulin/IGF-1 reduction and *eat-2* associated effects are accompanied by distinct, yet partially independent, changes in the proteostasis network, particularly in folding (linked to both insulin/IGF-1 reduction and dietary restriction) and antioxidant responses (linked to insulin/IGF-1 reduction). However, mechanistic alterations in the heat shock response (HSR) are common to both pathways and may be key in explaining their shared modifying effects on motor phenotype. Moreover, the study puts forward innovative therapeutic approaches, such as repurposing cancer-related drugs targeting the insulin/IGF-1 pathway, as a potential strategy to be investigated for treating neurodegenerative diseases.

5. Star methods

REAGENT or RESOURCE	SOURCE	IDENTIFIER
Antibodies		
anti-ATXN3 mouse	Millipore	MAB5360
HRP-conjugated Secondary Antibody	Biorad	0300–0108 P
Chemicals, Peptides, and Recombinant Proteins		
Levamisole	Sigma-Aldrich	L9756
Trizol	Invitrogen	15596026
Chloroform	Sigma-Aldrich	C2432
Isopropanol	Honeywell	33539
Ethanol	Honeywell	4146052
DNAse I	Thermo Scientific	EN0521
iScript™ cDNA Synthesis Kit	Biorad	1708891
5x HOT FIREPol® EvaGreen® qPCR Mix Plus (ROX)	Solis BioDyne	08–24–00020
5-Hydroxy−1,4-naphthoquinone	Sigma-Aldrich	H47003
Ampicilin	Sigma-Aldrich	A9518
Isopropyl β-D−1-thiogalactopyranoside	Sigma-Aldrich	I5502
Penicillin-Streptomycin	Sigma-Aldrich	P4333
Nystatin	Sigma-Aldrich	N1638
EDTA-free proteases inhibitor cocktail	Roche	11836170001
Glass beads, acid-washed	Sigma-Aldrich	G8772
Bacterial and Virus strains		
Escherichia coli: Strain OP50	CGC	OP50
Experimental Models: Organisms/Strains		
N2 Bristol strain	CGC	N2
clk−1 (e2519) III	CGC	CB487
isp−1 (qm150) IV	CGC	MQ887
eat−2 (ad1113) II	CGC	DA1113
daf−2 (e1370) III	CGC	CB1370
glp−1 (e2144) III	CGC	CF1903
mIS263 [PF25B3.3::AT3v1–1q130::yfp]	Patricia Maciel Lab	AM685 (H10 line)
mIS263 [PF25B3.3::AT3v1–1q130::yfp]	Patricia Maciel Lab	AM599 (P5 line)
clk−1 (qm30) III; mIS263 [PF25B3.3::AT3v1–1q130::yfp]	This study	MQ130; AM685
isp−1 (qm150) IV;mIS263 [PF25B3.3::AT3v1–1q130::yfp]	This study	CB4876; AM685
eat−2 (ad1113) II;mIS263 [PF25B3.3::AT3v1–1q130::yfp]	This study	DA1113; AM599
daf−2 (e1370) III;mIS263 [PF25B3.3::AT3v1–1q130::yfp]	This study	CB1370; AM685
glp−1 (e2144) III;mIS263 [PF25B3.3::AT3v1–1q130::yfp]	This study	CF1903; AM685
wuIs151 [ctl−1(+) + ctl−2(+) + ctl−3 (+) + myo−2p::GFP]	CGC	GA800
wuIs151 [ctl−1(+) + ctl−2(+) + ctl−3 (+) + myo−2p::GFP]; mIS263 [PF25B3.3::AT3v1–1q130::yfp]	This study	GA800; AM685
Oligonucleotides		
See Table S2 for all primer sequences	N/A	N/A
Software and Algorithms		
Mevislab	[(Teixeira-Castro et al., 2011b)]	N/A

5.1. Lead contact

Further information and requests for resources and reagents should be directed to and will be fulfilled by the Lead Contact, Marta Daniela Costa (martacosta@med.uminho.pt)

5.2. Materials availability

There are no restrictions to the availability of *C. elegans* strains generated in this study. These strains are available upon request.

5.3. Data and code availability

The datasets supporting the current study have not been deposited in a public repository but are available from the corresponding author on request.

5.4. Experimental model and subject details

5.4.1. C. elegans strains and growth conditions

The strains used in this work, including the double mutants generated for the experiments, are listed in the Key Resources Table. All strains were backcrossed to Bristol strain N2 five to eight times. The MJD/SCA3 double mutants were generated by crossing different long-lived strains with the transgenic AT3q130 model (AM685, H10 line). Only the DA1113 (*eat-2* mutation) strain was crossed with a different line of AT3q130 model (P5 line), to circumvent chromosomal co-

localization of genetic alterations. Of note, in all experiments the eat-2 double mutants are compared with the P5 transgenic line, which has a milder phenotype than the H10 at baseline. *C. elegans* strains were cultured under standard procedures, on NGM plates seeded with *E. coli* (OP50), at 20ºC, except for the experiments involving the germline-deficient strains and the respective controls (bearing a *glp-1 (e2144)* genetic alteration), for which the temperature of maintenance was 15ºC, with an upshift to 25ºC early in development to arrest germline proliferation, leading to sterility.

5.5. Method details

5.5.1. Synchronization of C. elegans strains

For all experiments, synchronized populations of *C. elegans* were obtained using two techniques: 1) Egg-laying: gravid adult worms were let in plates for 2–4 h laying eggs which will constitute the synchronized worm population; 2) Bleaching methodology: gravid worms were treated with diluted alkaline hypochlorite solution (0.5 M NaOH, ~2.6 % NaClO) for 5–7 minutes. The resultant eggs were incubated overnight in M9 buffer and the hatched L1 larvae were then transferred to NGM plates seeded with OP50. For the strains with normal development, four-days old animals were considered as day 1 adults. The lethargic strains bearing *clk-1*, *isp-1* and *daf-2* mutations were synchronized ~1 day before the strains with normal development to guarantee that populations evaluated in the different assays were in the same developmental stage.

5.5.2. Lifespan assay

Lifespan assays were performed in NGM plates seeded with inactivated OP50 bacteria (through 3 freeze/thaw cycles in liquid nitrogen followed by water bath at 37ºC). Animals were grown in NGM seeded plates from L1 and lifespan assay started by plating 100 L4 animals per condition (day 0). Animals were transferred daily to freshly seeded plates in the first two weeks and every 2 days for the remainder of the assay. The scoring of dead animals occurred daily; an animal being considered dead if no mechanical response was elicited upon 3 light touches on its head with a platinum wire. Censoring was considered if internal hatching, extrusion of coelomic content or desiccation in the border of the plate had been noticed. Assays were performed independently, at least two times. Representative data are shown on survival graphs.

5.5.3. Motility assay

The motility tests were performed in synchronized worm populations, at day 2 or day 4 od adulthood (details mentioned in figure captions). Motility assays were performed at 20º C as previously described (Teixeira-Castro et al., 2011a). Briefly, five to ten animals were placed simultaneously in the middle of a freshly seeded plate. Animals remaining inside a 1 cm circle after 1 minute were considered locomotion defective. All assays were performed independently three or four times and 50 animals per genotype were tested in each assay.

5.5.4. Quantification of mutant ATXN3 aggregation

Measurement of mutant ATXN3 aggregation in the animals' heads was performed through confocal dynamic imaging on an Olympus FV1000 (Japan) confocal microscope, under a × 60 oil (NA = 1.35) objective. Animals originated from the same population were immobilized with 5–10 mM levamisole and mounted on a 5 % agarose pad, at days 4, 5, and 7 of adulthood. For all strains, images were acquired on Z-series imaging using a 515 nm laser excitation line. The pinhole was adjusted to 1.0 Airy unit of optical slice, and a scan was acquired every ~0.5 mm along the z-axis. The quantification of the aggregates was performed on an image processing tool using MeVislab as a platform, as previously described (Teixeira-Castro et al., 2011a, 2011b). Confocal images were used to measure the following parameters: 1) number of aggregates/total head area and 2) area of aggregates/total head area. At least two independent assays were performed for each condition; 6–8 images were obtained per genotype.

5.6. SDS-page and western-blot analysis

For determination of the steady-state protein levels of ATXN3, animals were collected at day 2 of adulthood and washed three times with M9, followed by flash-freezing in liquid nitrogen. After extraction with 50 μl of non-denaturating protein buffer (50 mM HEPES, pH 7.4, 150 mM NaCl, 1 mM EDTA, 0.5 % Triton X-100) freshly supplemented with EDTA-free proteases inhibitor cocktail (Roche), worms were disrupted by mechanic force using glass beads and acid-washed in a FastPrep®-24 (MP Biomedicals) (six cycles of 6·5 ms for 45 s followed by 1 min on ice). After a centrifugation of 500 g during 1 min, the supernatant was collected, and the total protein quantified by the Bradford assay (Bio-Rad). 5 μg of total protein were transfer to an Eppendorf screw tube, supplemented with Laemmli Buffer to a 1x concentration and boiled for 15 minutes. The samples were resolved in a 10 % SDS-polyacrylamide gel. After transferring, the membrane was incubated with AzureRed Fluorescent Total Protein Stain (Azure Biosystems) as per the manufacturer's instructions. Immunoblots were probed with anti-ATXN3 mouse (1:1000) and detected with horseradish peroxidase-coupled secondary antibodies and chemiluminescence (Radiance ECL, Azure Biosystems). To capture the chemiluminescence signal, the Sapphire Biomolecular Imager (Azure Biosystems) was used and western blot quantifications were performed using AzureSpot Analysis Software (Azure Biosystems), according to the manufacturer's instructions.

5.7. Pharyngeal pumping

To quantify the number of pharyngeal pumps per minute, animals were picked to OP50 seeded plates and after 30 minutes, filmed for 15–20 seconds. The total number of terminal bulb grinder contractions was manually counted in 0.5x speed videos.

5.8. RNAi-mediated genetic silencing

HTT115 bacteria expressing cDNA for *eat-2*, *hsf-1* and for an empty vector (EV), were used as *C. elegans* food source to promote RNAi-mediated silencing. The bacterial clones were acquired from from Vidal and Ahringer libraries, respectively (Rual et al., 2004). NGM plates supplemented with ampicillin (100 μg/mL) and isopropyl β-D-1-thio-galactopyranoside (400 μM) were seeded with the respective bacterial clone (grown in LB with 100 μg/mL ampicillin) and dried immediately in camera laminar flow hood. Adult animals were plated to lay eggs for 2–3 h. The resultant synchronized population of worms was grown until day 2 or day 4 of adulthood.

5.9. Toxicity assay of IGF-1R tyrosine kinase inhibitor

The *C. elegans* Bristol strain N2 was used to evaluate the toxicity of IGF-1R tyrosine kinase inhibitor. The assay was performed as previously described, (Teixeira-Castro et al., 2015) in liquid culture and using 96-well flat plates. Each well contained a final volume of 60 μL: 15 μL of eggs suspension (20–25 eggs), 25 μL of each compound at different concentrations and 20 μL of OP50 bacteria (OD_{595} of 0.6–0.7). The OP50 bacteria was previously grown overnight at 37°C and 180 rpm in Luria Broth (LB) media, pelleted by centrifugation, inactivated by 3 cycles of freeze/thawing, frozen at −80°C and then resuspended in S-medium complete. Worms were grown with continuous shaking at 180 rpm at 20°C (Shell Lab incubator shaker) for 7 days. The consumption of OP50 was measured daily at 595 nm (NanoQuant Plate™-Tecan) and confirmation of normal development and healthy appearance was confirmed by visual inspection.

5.10. Treatment with IGF-1R tyrosine kinase inhibitor

Chronic treatment of the *C. elegans* strains with the IGF-1R tyrosine kinase inhibitor was performed in liquid culture (96-well flat plates) with 45–50 L1 animals per well in S-medium; IGF-1R tyrosine kinase inhibitor at distinct concentrations in DMSO 1 %; and inactivated OP50 bacteria resuspended in S-medium complete to a final OD_{595} of 0.8–0.9. The plates were sealed to prevent evaporation and incubated at 20°C with shaking at 180 rpm (Shell lab incubator shaker) until day 2 of adulthood.

5.10.1. Worm RNA extraction and cDNA synthesis

Day 2 of adulthood synchronized worms were pelleted and vortexed in 500 μL TRIzol®. A step of freeze/thawing followed by vortexing was performed to increment worm lysis. After 10 minutes at room temperature (RT), the tubes were centrifuged at 14,000 rpm for 10 minutes. The supernatant was transferred to a new tube and 100 μL chloroform was added. Tubes were vortexed for 15 seconds before centrifugation at 13,000 rpm for 15 minutes. The upper aqueous layer of supernatant was removed to a new tube and 500 μL isopropanol was added for 10 minutes before centrifugation at 12,000 rpm for 10 minutes. Supernatant was discarded and the pellet was washed in 70 % ethanol before centrifugation at 10,000 rpm for 5 minutes. The supernatant was discarded, and the pellet was air-dried before being dissolved in RNase-free water at 60ºC for 10 minutes. DNA contamination was reduced with DNAse I treatment, according to the manufacturer's protocol.

5.10.2. Quantitative real-time PCR

RNA was reverse-transcribed to complementary DNA using the iScript™ cDNA Synthesis Kit, according to the manufacturer's protocol. Quantitative PCR was performed in an Applied Bio Systems 7500 Real Time PCR System employing 5x HOT FIREPol® EvaGreen® qPCR Mix Plus (ROX). Gene expression data was normalized to housekeeping genes *pmp-3* and *rpb-2*. All data corresponded to at least three independent biological replicates, each comprising 2–4 technical repeats. Primers were designed in Primer-Blast (http://www.ncbi.nlm.nih.gov/tools/primer-blast/) and sequences are listed in the Key resources table. Primer efficiency was between 85 % and 110 %.

5.11. Juglone resistance assays

Synchronized L1 worms were allowed to develop at 20ºC up to day 4 after hatching. A 12 mM Juglone/5-Hydroxy-1,4-naphthoquinone 97 % (Sigma, Missouri, USA) solution was made freshly in 100 % ethanol and used 1 hour after preparation. The worms were collected from plates to falcons and washed 2 times in M9 buffer. A total of 200–400 animals were then transferred to 24-well plates in M9 buffer and a final concentration of 240 μM of juglone was added to each well. After 4 hours of treatment, the worms were collected and washed 4–5 times in M9 buffer and transferred to NGM solid plates seeded with OP50. The number of living worms was scored after a recovery period of 16 h.

5.12. Quantification and statistical analysis

Statistical analysis was performed using GraphPad Prism 7 and SPSS. All statistical details corresponding to each experiment, including the value of n, descriptive statistics (mean ± SEM or SD) and statistical significance, are described in figure captions. All continuous variables were tested for normality and homogeneity of variances. Outliers were evaluated and excluded from analysis of RT-qPCR data and for the results concerning the insulin/IGF-1 targeting drugs. For the comparison of means, the Student's *t*-test, One-way and Two-way analysis of variance (ANOVA) was applied, for the comparison of two and more than two means, respectively. In both cases, suitable corrections were assumed whenever homogeneity of variances was not guaranteed. If data were not normally distributed, non-parametric tests were used. Survival data was evaluated using a Cox regression model. Statistical analysis of mutATXN3 aggregation measures was performed using a Student *t*-test with Sidak's multiple comparison adjustment. For RT-qPCR data, a planned contrasts (orthogonal) analysis was performed in the one-way ANOVA, in order to maximize statistical power without significantly inflating the type I error rate. The following pairwise comparisons were performed in these analyses: N2-AT3q130; N2-single mutants; AT3q130-double mutants; single mutants-double mutants

CRediT authorship contribution statement

Almeida Dulce: Investigation. **Vilasboas-Campos Daniela:** Writing – review & editing, Investigation. **Pereira-Sousa Joana:** Writing – review & editing, Investigation. **Teixeira Castro Andreia:** Writing – review & editing, Validation, Investigation, Funding acquisition, Conceptualization. **Fernandes Jorge Humberto:** Writing – review & editing, Investigation. **Maciel Patricia:** Writing – review & editing, Supervision, Project administration, Funding acquisition. **da Silva Jorge:** Writing – review & editing, Validation, Investigation, Formal analysis. **Costa Marta Daniela:** Writing – original draft, Methodology, Investigation, Formal analysis, Data curation, Conceptualization.

Funding

This work has been funded by ICVS Scientific Microscopy Platform, member of the national infrastructure PPBI - Portuguese Platform of Bioimaging (PPBI-POCI-01–0145-FEDER-022122; and by National funds, through the Foundation for Science and Technology (FCT) - project UIDB/50026/2020 (DOI 10.54499/UIDB/50026/2020), UIDP/50026/2020 (DOI 10.54499/UIDP/50026/2020), LA/P/0050/2020 (DOI 10.54499/LA/P/0050/2020) and PTDC/NEU-BEN/0125/2012. Funding from FCT also supported the research scholarships to MDC (SFRH/BPD/101925/2014), JDDS (PD/BD/128074/2016), JHF (SFRH/BD/07314/2021), DVC (SFRH/BD/147826/2019) and to JPS (PD/BDE/127834/2016). ATC also received a project funded by FCT - 2023.15102.PEX. This work has been also funded by the National Ataxia Foundation (NAF) through grants given to MDC (Seed money 2018) and ATC (Early career investigator award 2024)

Declaration of Competing Interest

The authors declare no competing financial and non-financial interests.

Acknowledgments

The authors thank all members of the Maciel lab for the helpful suggestions and results discussion. We are also grateful to the Caenorhabditis Genetics Center (CGC), which is funded by the National Institutes of Health – National Center for Research Resources, for having provided some of the nematode strains and to Drs. Isabel Alonso, Maria Conceição Pereira and Mariana Graça for providing RNAi bacterial clones.

Appendix A. Supporting information

Supplementary data associated with this article can be found in the online version at doi:10.1016/j.mad.2025.112064.

Data availability

Data will be made available on request.

References

Antebi, A., 2013. Regulation of longevity by the reproductive system. Exp. Gerontol. 48, 596–602.

Arantes-Oliveira, N., Apfeld, J., Dillin, A., Kenyon, C., 2002. Regulation of life-span by germ-line stem cells in Caenorhabditis elegans. Science 295, 502–505.

Arcaro, A., 2013. Targeting the insulin-like growth factor-1 receptor in human cancer. Front. Pharmacol. 4.

Bettencourt, C., Lima, M., 2011. Machado-Joseph disease: from first descriptions to new perspectives. Orphanet J. rare Dis. 6, 35.

Blackwell, T.K., Steinbaugh, M.J., Hourihan, J.M., Ewald, C.Y., Isik, M., 2015. SKN-1/Nrf, stress responses, and aging in Caenorhabditis elegans. Free Radic. Biol. Med. 88, 290–301.

Cohen, E., Bieschke, J., Perciavalle, R.M., Kelly, J.W., Dillin, A., 2006. Opposing activities protect against age-onset proteotoxicity. Science 313, 1604–1610.

Cooper, J.F., Dues, D.J., Spielbauer, K.K., Machiela, E., Senchuk, M.M., Van Raamsdonk, J.M., 2015. Delaying aging is neuroprotective in Parkinson's disease: a genetic analysis in C. elegans models. npj Park. 'S. Dis. 1, 15022.

Doonan, R., McElwee, J.J., Matthijssens, F., Walker, G.A., Houthoofd, K., Back, P., Matscheski, A., Vanfleteren, J.R., Gems, D., 2008. Against the oxidative damage theory of aging: superoxide dismutases protect against oxidative stress but have little or no effect on life span in Caenorhabditis elegans. Genes Dev. 22, 3236–3241.

El-Ami, T., Moll, L., Carvalhal Marques, F., Volovik, Y., Reuveni, H., Cohen, E., 2014. A novel inhibitor of the insulin/IGF signaling pathway protects from age-onset, neurodegeneration-linked proteotoxicity. Aging Cell 13, 165–174.

Fan, H.C., Ho, L.I., Chi, C.S., Chen, S.J., Peng, G.S., Chan, T.M., Lin, S.Z., Harn, H.J., 2014. Polyglutamine (PolyQ) diseases: genetics to treatments. Cell Transplant. 23, 441–458.

Feng, J., Bussière, F., Hekimi, S., 2001. Mitochondrial electron transport is a key determinant of life span in Caenorhabditis elegans. Dev. Cell 1, 633–644.

Gao, A.W., Smith, R.L., van Weeghel, M., Kamble, R., Janssens, G.E., Houtkooper, R.H., 2018. Identification of key pathways and metabolic fingerprints of longevity in C. elegans. Exp. Gerontol. 113, 128–140.

Goudeau, J., Bellemin, S., Toselli-Mollereau, E., Shamalnasab, M., Chen, Y., Aguilaniu, H., 2011. Fatty acid desaturation links germ cell loss to longevity through NHR-80/HNF4 in C. elegans. PLoS Biol. 9, e1000599.

Haisa, M., 2013. The type 1 insulin-like growth factor receptor signalling system and targeted tyrosine kinase inhibition in cancer. J. Int. Med. Res. 41, 253–264.

Harman, D., 2003. The free radical theory of aging. Antioxid. Redox Signal. 5, 557–561.

Hou, Y., Dan, X., Babbar, M., Wei, Y., Hasselbalch, S.G., Croteau, D.L., Bohr, V.A., 2019. Ageing as a risk factor for neurodegenerative disease. Nat. Rev. Neurol. 15, 565–581.

Hsin, H., Kenyon, C., 1999. Signals from the reproductive system regulate the lifespan of C. elegans. Nature 399, 362–366.

Hwang, A.B., Lee, S.J., 2011. Regulation of life span by mitochondrial respiration: the HIF-1 and ROS connection. Aging 3, 304–310.

Kenyon, C., Chang, J., Gensch, E., Rudner, A., Tabtiang, R., 1993. A C. elegans mutant that lives twice as long as wild type. Nature 366, 461–464.

Kenyon, C.J., 2010. The genetics of ageing. Nature 464, 504–512.

King, E.R., Wong, K.-K., 2012. Insulin-like growth factor: current concepts and new developments in cancer therapy. Recent Pat. Anticancer Drug Discov. 7, 14–30.

Kumar, S., Egan, B.M., Kocsisova, Z., Schneider, D.L., Murphy, J.T., Diwan, A., Kornfeld, K., 2019. Lifespan Extension in C. elegans Caused by Bacterial Colonization of the Intestine and Subsequent Activation of an Innate Immune Response. Dev. Cell 49, 100–117 e106.

Lee, J.-Y., Kawaguchi, Y., Li, M., Kapur, M., Choi, S.J., Kim, H.-J., Park, S.-Y., Zhu, H., Yao, T.-P., 2015. Uncoupling of Protein Aggregation and Neurodegeneration in a Mouse Amyotrophic Lateral Sclerosis Model. Neurodegener. Dis. 15, 339–349.

Lee, S.J., Hwang, A.B., Kenyon, C., 2010. Inhibition of respiration extends C. elegans life span via reactive oxygen species that increase HIF-1 activity. Curr. Biol.: CB 20, 2131–2136.

Lee, S.S., Lee, R.Y., Fraser, A.G., Kamath, R.S., Ahringer, J., Ruvkun, G., 2003. A systematic RNAi screen identifies a critical role for mitochondria in C. elegans longevity. Nat. Genet 33, 40–48.

Lieberman, A.P., Shakkottai, V.G., Albin, R.L., 2019. Polyglutamine Repeats in Neurodegenerative Diseases. Annu. Rev. Pathol. 14, 1–27.

Maciel, P., Gaspar, C., DeStefano, A.L., Silveira, I., Coutinho, P., Radvany, J., Dawson, D. M., Sudarsky, L., Guimaraes, J., Loureiro, J.E., et al., 1995. Correlation between CAG repeat length and clinical features in Machado-Joseph disease. Am. J. Hum. Genet. 57, 54–61.

Mair, W., Dillin, A., 2008. Aging and survival: the genetics of life span extension by dietary restriction. Annu. Rev. Biochem. 77, 727–754.

Matai, L., Sarkar, G.C., Chamoli, M., Malik, Y., Kumar, S.S., Rautela, U., Jana, N.R., Chakraborty, K., Mukhopadhyay, A., 2019. Dietary restriction improves proteostasis and increases life span through endoplasmic reticulum hormesis. Proc. Natl. Acad. Sci. 116, 17383–17392.

McCay, C.M., Crowell, M.F., Maynard, L.A., 1989. The effect of retarded growth upon the length of life span and upon the ultimate body size. 1935. Nutrition 5, 155–171 discussion 172.

Morley, J.F., Brignull, H.R., Weyers, J.J., Morimoto, R.I., 2002. The threshold for polyglutamine-expansion protein aggregation and cellular toxicity is dynamic and influenced by aging in Caenorhabditis elegans. Proc. Natl. Acad. Sci. USA 99, 10417–10422.

Murphy, C.T., Hu, P.J., 2013. Insulin/insulin-like growth factor signaling in C. elegans. WormBook: Online Rev. C. elegans Biol. 1–43.

O'Rourke, E.J., Ruvkun, G., 2013. MXL-3 and HLH-30 transcriptionally link lipolysis and autophagy to nutrient availability. Nat. Cell Biol. 15, 668–676.

Panowski, S.H., Wolff, S., Aguilaniu, H., Durieux, J., Dillin, A., 2007. PHA-4/Foxa mediates diet-restriction-induced longevity of C. elegans. Nature 447, 550–555.

Paulson, H., 2012. Machado-Joseph disease/spinocerebellar ataxia type 3. Handb. Clin. Neurol. 103, 437–449.

Pohl, F., Teixeira-Castro, A., Costa, M.D., Lindsay, V., Fiúza-Fernandes, J., Goua, M., Bermano, G., Russell, W., Maciel, P., Kong Thoo Lin, P., 2019. GST-4-dependent suppression of neurodegeneration in C. elegans models of Parkinson's and Machado-Joseph disease by rapeseed pomace extract supplementation. Front Neurosci. 13, 1091–10911.

Qin, Z., Hubbard, E.J., 2015. Non-autonomous DAF-16/FOXO activity antagonizes age-related loss of C. elegans germline stem/progenitor cells. Nat. Commun. 6, 7107.

Ratnappan, R., Amrit, F.R., Chen, S.W., Gill, H., Holden, K., Ward, J., Yamamoto, K.R., Olsen, C.P., Ghazi, A., 2014. Germline signals deploy NHR-49 to modulate fatty-acid β-oxidation and desaturation in somatic tissues of C. elegans. PLoS Genet 10, e1004829.

Rual, J.-F., Ceron, J., Koreth, J., Hao, T., Nicot, A.-S., Hirozane-Kishikawa, T., Vandenhaute, J., Orkin, S.H., Hill, D.E., van den Heuvel, S., et al., 2004. Toward improving caenorhabditis elegans phenome mapping With an ORFeome-based RNAi library. Genome Res. 14, 2162–2168.

Senchuk, M.M., Dues, D.J., Schaar, C.E., Johnson, B.K., Madaj, Z.B., Bowman, M.J., Winn, M.E., Van Raamsdonk, J.M., 2018. Activation of DAF-16/FOXO by reactive oxygen species contributes to longevity in long-lived mitochondrial mutants in Caenorhabditis elegans. PLoS Genet. 14, e1007268–e10072618.

Senchuk, M.M., Van Raamsdonk, J.M., Moore, D.J., 2021. Multiple genetic pathways regulating lifespan extension are neuroprotective in a G2019S LRRK2 nematode model of Parkinson's disease. Neurobiol. Dis. 151, 105267.

Steinkraus, K.A., Smith, E.D., Davis, C., Carr, D., Pendergrass, W.R., Sutphin, G.L., Kennedy, B.K., Kaeberlein, M., 2008. Dietary restriction suppresses proteotoxicity and enhances longevity by an hsf-1-dependent mechanism in Caenorhabditis elegans. Aging Cell 7, 394–404.

Tank, E.M., Rodgers, K.E., Kenyon, C., 2011. Spontaneous age-related neurite branching in Caenorhabditis elegans. J. Neurosci. 31, 9279–9288.

Teixeira-Castro, A., Ailion, M., Jalles, A., Brignull, H.R., Vilaça, J.L., Dias, N., Rodrigues, P., Oliveira, J.F., Neves-Carvalho, A., Morimoto, R.I., et al., 2011a. Neuron-specific proteotoxicity of mutant ataxin-3 in C. elegans: rescue by the DAF-16 and HSF-1 pathways. Hum. Mol. Genet. 20, 2996–3009.

Teixeira-Castro, A., Dias, N., Rodrigues, P., Oliveira, J.F., Rodrigues, N.F., Maciel, P., and Vilaça, J.L. (2011b). An Image Processing Application for Quantification of Protein Aggregates in Caenorhabditis elegans. In 5th International Conference on Practical Applications of Computational Biology & Bioinformatics (PACBB 2011), M.P. Rocha, J.M.C. Rodríguez, F. Fdez-Riverola, andA. Valencia, eds. (Berlin, Heidelberg, Springer Berlin Heidelberg), pp 31-38.

Teixeira-Castro, A., Jalles, A., Esteves, S., Kang, S., da Silva Santos, L., Silva-Fernandes, A., Neto, M.F., Brielmann, R.M., Bessa, C., Duarte-Silva, S., et al., 2015. Serotonergic signalling suppresses ataxin 3 aggregation and neurotoxicity in animal models of Machado-Joseph disease. Brain: a J. Neurol. 138, 3221–3237.

Tullet, J.M., Hertweck, M., An, J.H., Baker, J., Hwang, J.Y., Liu, S., Oliveira, R.P., Baumeister, R., Blackwell, T.K., 2008. Direct inhibition of the longevity-promoting factor SKN-1 by insulin-like signaling in C. elegans. Cell 132, 1025–1038.

Uno, M., Nishida, E., 2016. Lifespan-regulating genes in C. elegans. npj Aging Mech. Dis. 2, 16010.

Wu, Z., Isik, M., Moroz, N., Steinbaugh, M.J., Zhang, P., Blackwell, T.K., 2019. Dietary restriction extends lifespan through metabolic regulation of innate immunity. Cell Metab. 29, 1192–1205 e1198.

Xue, M., Cao, X., Zhong, Y., Kuang, D., Liu, X., Zhao, Z., Li, H., 2012. Insulin-like growth factor-1 receptor (IGF-1R) kinase inhibitors in cancer therapy: advances and perspectives. Curr. Pharm. Des. 18, 2901–2913.

Yin, J.-A., Liu, X.-J., Yuan, J., Jiang, J., Cai, S.-Q., 2014. Longevity manipulations differentially affect serotonin/dopamine level and behavioral deterioration in aging Caenorhabditis elegans. J. Neurosci.: Off. J. Soc. Neurosci. 34, 3947–3958.

Yoneda, T., Benedetti, C., Urano, F., Clark, S.G., Harding, H.P., Ron, D., 2004. Compartment-specific perturbation of protein handling activates genes encoding mitochondrial chaperones. J. Cell Sci. 117, 4055–4066.

Zhang, T., Mullane, P.C., Periz, G., Wang, J., 2011. TDP-43 neurotoxicity and protein aggregation modulated by heat shock factor and insulin/IGF-1 signaling. Hum. Mol. Genet. 20, 1952–1965.

Zhao, Q., Wang, J., Levichkin, I.V., Stasinopoulos, S., Ryan, M.T., Hoogenraad, N.J., 2002. A mitochondrial specific stress response in mammalian cells. EMBO J. 21, 4411–4419.